Research Article | Vol. 9, No. 3 | 1 Mar 2018 | BIOMEDICAL OPTICS EXPRESS 1190
Biomedical Optics EXPRESS

Optical resolution photoacoustic microscopy based on multimode fibers

MOHESH MOOTHANCHERY,[1,3] RENZHE BI[1,3] JIN YOUNG KIM,[2] SEUNGWAN JEON,[2] CHULHONG KIM,[2,4] MALINI OLIVO[1,5]

[1]*Singapore Bioimaging Consortium, Agency for Science Technology and Research (A*STAR), 11 Biopolis Way, Singapore, 138667, Singapore*
[2]*Department of Creative IT Engineering, Pohang University of Science and Technology (POSTECH), Pohang, 37673, South Korea*
[3]*Both authors contributed equally*
[4]*chulhong@postech.edu*
[5]*malini_olivo@sbic.a-star.edu.sg*

Abstract: Photoacoustic microscopy (PAM) is a multiscale imaging technique. In optical-resolution photoacoustic microscopy (OR-PAM), a single mode (SM) fiber is normally used as the source of optical excitation to be focused into a diffraction-limited spot. Recent advances in OR-PAM have improved its imaging speed using microelectromechanical systems (MEMS). Here we report for the first time the use of a multimode (MM) fiber as the optical excitation source for high resolution OR-PAM *in vivo* imaging. A high-speed MEMS scanner based OR-PAM system combined with the mechanical movement to provide wide area imaging was used. The use of multimode fiber for achieving tight optical focus would make the optical alignment easier and high repetition rate light delivery possible for high-speed OR-PAM imaging. A lateral resolution of 3.5 µm and axial resolution of 27 µm with ~1.5 mm imaging depth was successfully demonstrated using the system. The efficacy of multimode fibers for achieving tight focus is beneficial for developing high-resolution photoacoustic endoscopy systems and can be combined with other optical endoscopic imaging modalities as well.

OCIS codes: (110.5120) Photoacoustic imaging; (110.5125) Photoacoustics; (170.0180) Microscopy.

References and links

1. L. V. Wang and J. Yao, "A practical guide to photoacoustic tomography in the life sciences," Nat. Methods **13**(8), 627–638 (2016).
2. Y. Zhou, J. Yao, and L. V. Wang, "Tutorial on photoacoustic tomography," J. Biomed. Opt. **21**(6), 061007 (2016).
3. J. Yao and L. V. Wang, "Photoacoustic Brain Imaging: from Microscopic to Macroscopic Scales," Neurophotonics **1**(1), 011003 (2014).
4. L. V. Wang and S. Hu, "Photoacoustic Tomography: In Vivo Imaging from Organelles to Organs," Science **335**(6075), 1458–1462 (2012).
5. P. Beard, "Biomedical photoacoustic imaging," Interface Focus **1**(4), 602–631 (2011).
6. L. V. Wang, "Multiscale photoacoustic microscopy and computed tomography," Nat. Photonics **3**(9), 503–509 (2009).
7. E. Z. Zhang, J. G. Laufer, R. B. Pedley, and P. C. Beard, "In vivo high-resolution 3D photoacoustic imaging of superficial vascular anatomy," Phys. Med. Biol. **54**(4), 1035–1046 (2009).
8. M. Moothanchery and M. Pramanik, "Performance Characterization of a Switchable Acoustic Resolution and Optical Resolution Photoacoustic Microscopy System," Sensors (Basel) **17**(2), 357 (2017).
9. M. Moothanchery, R. Z. Seeni, C. Xu, and M. Pramanik, "In vivo studies of transdermal nanoparticle delivery with microneedles using photoacoustic microscopy," Biomed. Opt. Express **8**(12), 5483–5492 (2017).
10. S. Park, C. Lee, J. Kim, and C. Kim, "Acoustic resolution photoacoustic microscopy," Biomed. Eng. Lett. **4**(3), 213–222 (2014).
11. H. F. Zhang, K. Maslov, G. Stoica, and L. V. Wang, "Functional photoacoustic microscopy for high-resolution and noninvasive in vivo imaging," Nat. Biotechnol. **24**(7), 848–851 (2006).
12. K. Maslov, G. Stoica, and L. V. Wang, "In vivo dark-field reflection-mode photoacoustic microscopy," Opt. Lett. **30**(6), 625–627 (2005).

#313892 https://doi.org/10.1364/BOE.9.001190
Journal © 2018 Received 20 Nov 2017; revised 16 Jan 2018; accepted 18 Jan 2018; published 15 Feb 2018

Biomedical Optics EXPRESS

13. W. Song, W. Zheng, R. Liu, R. Lin, H. Huang, X. Gong, S. Yang, R. Zhang, and L. Song, "Reflection-mode in vivo photoacoustic microscopy with subwavelength lateral resolution," Biomed. Opt. Express **5**(12), 4235–4241 (2014).
14. S. Hu, K. Maslov, and L. V. Wang, "Second-generation optical-resolution photoacoustic microscopy with improved sensitivity and speed," Opt. Lett. **36**(7), 1134–1136 (2011).
15. M. Moothanchery, A. Sharma, and M. Pramanik, "Switchable Acoustic and Optical Resolution Photoacoustic Microscopy for in vivo small-animal blood vasculature imaging," J. Vis. Exp. **124**, e55810 (2017).
16. S. Jeon, H. B. Song, J. Kim, B. J. Lee, R. Managuli, J. H. Kim, J. H. Kim, and C. Kim, "In Vivo Photoacoustic Imaging of Anterior Ocular Vasculature: A Random Sample Consensus Approach," Sci. Rep. **7**(1), 4318 (2017).
17. J. Yao, C.-H. Huang, L. Wang, J.-M. Yang, L. Gao, K. I. Maslov, J. Zou, and L. V. Wang, "Wide-field fast-scanning photoacoustic microscopy based on a water-immersible MEMS scanning mirror," J. Biomed. Opt. **17**(8), 080505 (2012).
18. J. Y. Kim, C. Lee, K. Park, G. Lim, and C. Kim, "Fast optical-resolution photoacoustic microscopy using a 2-axis water-proofing MEMS scanner," Sci. Rep. **5**(1), 7932 (2015).
19. K. Park, J. Y. Kim, C. Lee, S. Jeon, G. Lim, and C. Kim, "Handheld Photoacoustic Microscopy Probe," Sci. Rep. **7**(1), 13359 (2017).
20. J.-M. Yang, R. Chen, C. Favazza, J. Yao, C. Li, Z. Hu, Q. Zhou, K. K. Shung, and L. V. Wang, "A 2.5-mm diameter probe for photoacoustic and ultrasonic endoscopy," Opt. Express **20**(21), 23944–23953 (2012).
21. Y. Yuan, S. Yang, and D. Xing, "Preclinical photoacoustic imaging endoscope based on acousto-optic coaxial system using ring transducer array," Opt. Lett. **35**(13), 2266–2268 (2010).
22. I. N. Papadopoulos, O. Simandoux, S. Farahi, J. P. Huignard, E. Bossy, D. Psaltis, and C. Moser, "Optical-resolution photoacoustic microscopy by use of a multimode fiber," Appl. Phys. Lett. **102**(21), 211106 (2013).
23. M. Hughes, T. P. Chang, and G.-Z. Yang, "Fiber bundle endocytoscopy," Biomed. Opt. Express **4**(12), 2781–2794 (2013).
24. M. Hughes and G.-Z. Yang, "High speed, line-scanning, fiber bundle fluorescence confocal endomicroscopy for improved mosaicking," Biomed. Opt. Express **6**(4), 1241–1252 (2015).
25. R. Y. Gu, R. N. Mahalati, and J. M. Kahn, "Design of flexible multi-mode fiber endoscope," Opt. Express **23**(21), 26905–26918 (2015).
26. S. Turtaev, T. Leite Ivo, and T. Čižmár, "Multimode fibres for micro-endoscopy," in *Optofluidics, Microfluidics and Nanofluidics,* (deGruyer, 2015), p. 31.
27. T. Čižmár and K. Dholakia, "Exploiting multimode waveguides for pure fibre-based imaging," Nat. Commun. **3**, 1027 (2012).
28. P. Shao, W. Shi, P. Hajireza, and R. J. Zemp, "Integrated micro-endoscopy system for simultaneous fluorescence and optical-resolution photoacoustic imaging," J. Biomed. Opt. **17**(7), 076024 (2012).

1. Introduction

Photoacoustic microscopy (PAM) is an emerging innovative hybrid *in vivo* imaging modality, which combines optical absorption contrast and ultrasonic resolution [1–9]. In PAM, a short pulsed laser will irradiate the sample to generate acoustic waves due to the temperature rise induced by the sample. The acoustic waves can be detected by an ultrasonic transducer outside the sample. Depending on the resolution and imaging depth, PAM can be classified as acoustic resolution photoacoustic microscopy (AR-PAM) and optical resolution photoacoustic microscopy (OR-PAM). In AR-PAM, taking advantage of weak optical and tight acoustic focusing deep tissue imaging was achieved [10–12]. A lateral resolution of 45 μm and imaging depth up to 3 mm was reported using a 50 MHz focused ultrasound transducer having a numerical aperture (NA) of 0.44. Acoustically resolving single capillaries needs ultrasonic transducers having a center frequency greater than 400 MHz. The penetration depth at these higher frequencies will be less than 100 μm. Tight optical focusing will further improve the lateral resolution for PAM and resolution up to 0.32 μm has been reported using OR-PAM [13]. The imaging depth in OR-PAM is limited by optical transport mean free path (~1 mm inside the biological tissue) [14–16]. In OR-PAM, the optical delivery is mainly through a SM fiber. Single mode fiber coupling is complicated and often damage the fiber due to poor coupling and lower fiber damage threshold. MEMS based scanning has been proposed previously in order to improve the scanning speed for OR-PAM [17–19], however delivering nanosecond pulses at high repetition rates using SM fibers is rather difficult to achieve because of its lower damage threshold.

In order to overcome the imaging depth limitations of OR-PAM, progress has already been made in miniaturizing the imaging modality as endoscopic devices [20, 21]. In photoacoustic endoscopy (PAE) a single mode fiber beam delivery system integrated with a

Biomedical Optics EXPRESS

transducer will be scanned around the axis of the endoscope. The proposed PAE device have a poor lateral resolution of 58 µm. Focusing light beam through a multimode fiber for high resolution photoacoustic endoscopic applications was previously reported using optical phase conjugation technique [22] which however have a limited microscopic field of view. In pure optical endoscopic imaging modalities like confocal and fluorescence endoscopy, single mode fiber bundles were used [23, 24]. The imaging resolution of the system will depend on the spacing between each individual fiber core. Recently the use of multimode fibers for pure optical endoscopic imaging modalities was demonstrated which further reduced the footprint of the endoscopic devices as well as improved the imaging resolution and collection efficiency of the detected signals [25, 26]. Same multimode fiber can be used for optical excitation and signal collection in pure fiber-based fluorescence imaging [27]. An integrated micro-endoscopy system based on an image-guided fiber bundle for simultaneous optical resolution photoacoustic and fluorescence imaging was reported previously [28]. The use of a single multimode fiber for both photoacoustic and fluorescence endoscopic imaging would be highly beneficial to take the multimodal endoscopic technology forward.

Here we propose the use of multimode fibers for achieving diffraction limited optical focusing for OR-PAM high speed imaging applications. The use of MM fiber will make the optical alignment easier and light delivery more effectively for OR-PAM imaging, compared to SM fiber. Multimode fibers have higher damage threshold, hence would also be ideal for high repetition rate light delivery for high-speed OR-PAM imaging. The use of MM fibers can make the way for developing high-resolution PAE system and is advantageous for combining PAE with other optical endoscopic imaging modalities as well.

2. System description

Figure 1 shows the schematic of the OR-PAM system. The system employs a nanosecond pulsed laser (AWAVE-VIS-532, Advanced Optowave, USA) which can operate at a repetition rate of 5 kHz to 100 kHz. The laser beam passed through a combination of lenses, L1 and L2 (LD2297 and LA1509, Thorlabs). The collimated laser beam was attenuated by a neutral density filter, NDF (NDC-50C-4M, Thorlabs) and reshaped by an iris (ID12/M, Thorlabs). The beam was coupled to a multimode fiber, MMF (M64L01, Thorlabs) using a fiber coupler, FC (F240FC-532) placed in a kinematic mount (KC1-S/M, Thorlabs). A pair of achromatic lens, L3, L4 (32-317, Edmund Optics) was used to collimate and focus the output beam from the MMF. The optical and acoustic focus is aligned confocally through the optoacoustic beam combiner consisting of a combination of an aluminum-coated prism (NT32-331, Edmund Optics) and uncoated prism (NT32- 330, Edmund Optics). The aluminum coating provides acoustic transmission and optical reflection. The laser beam is focused onto the sample after being deflected by the aluminum coating of the combiner and then by the MEMS scanner. A correction lens (NT67-147, Edmund Optics) was attached to the top of the combiner for optical aberration corrections. An acoustic lens with an NA of 0.25 (NT45-010, Edmund Optics) was attached to the right side of the combiner which can provide an acoustic focal spot size of ~80 µm. The photoacoustic waves generated from the sample are initially reflected by the MEMS scanner then detected by an ultrasonic transducer (V214-BC-RM, Olympus-NDT) attached to the left side of the combiner. The detected signals were amplified by two serially connected amplifiers (ZX60-3018G + , Mini-Circuits) each having a 23 dB gain. A high-speed digitizer finally acquires these signals. The confocally and coaxially aligned light focus and acoustic focus scan the sample surface along the X-Y plane. The X-axis scanning was done using MEMS scanner (PAMsTECH, Republic of Korea). The MEMS scanner has a scanning limitation of 2 mm in both X and Y direction. For imaging area larger than 2 mm, we use MEMS scanner for capturing signals along the X-direction whereas the Y movement was done using mechanical stage. We have used a commercial PAM system (Microphotoacoustics, USA) for raster scanning and data acquisition.

Biomedical Optics EXPRESS

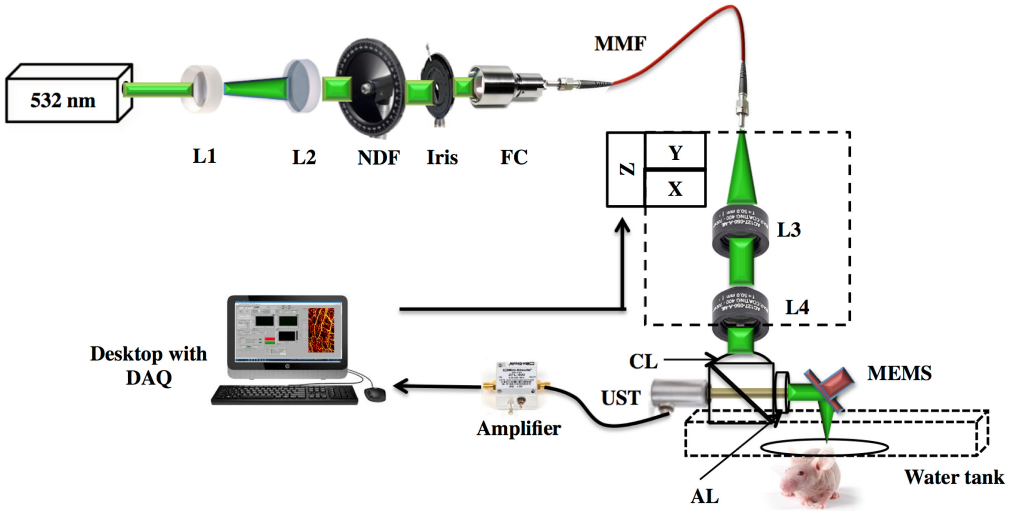

Fig. 1. (a) Schematic of the OR-PAM imaging system. L1- Bi-Concave lens, L2- Plano convex lens, NDF- Neutral density filter, FC - Fiber coupler, UST - Ultrasound transducer, MMF - Multimode fiber, DAQ - Data acquisition card, L3 & L4 - Achromatic lens, CL- Correction lens, AL - Acoustic lens.

3. Results and discussion

The performance of the high-speed OR-PAM system was quantified in terms of spatial resolution, maximum imaging depth and *in vivo* imaging. The lateral resolution of the OR-PAM system was determined using an Air Force resolution test target. Figure 2(a) shows the maximum amplitude projection (MAP) OR-PAM imaging carried on a 1.2 mm × 1.2 mm area of a USAF 1951 test target (R1DS1P, Thorlabs). The scan step size was 1.5 µm in the X and Y directions. Figure 2(b) shows a 230 µm × 230 µm area MAP OR-PAM image of the white dotted region in Fig. 3(a) with a step size of 1 µm. As from Fig. 3(b), we can see OR-PAM system can resolve 3.48 µm line pairs (group 7, element 2).

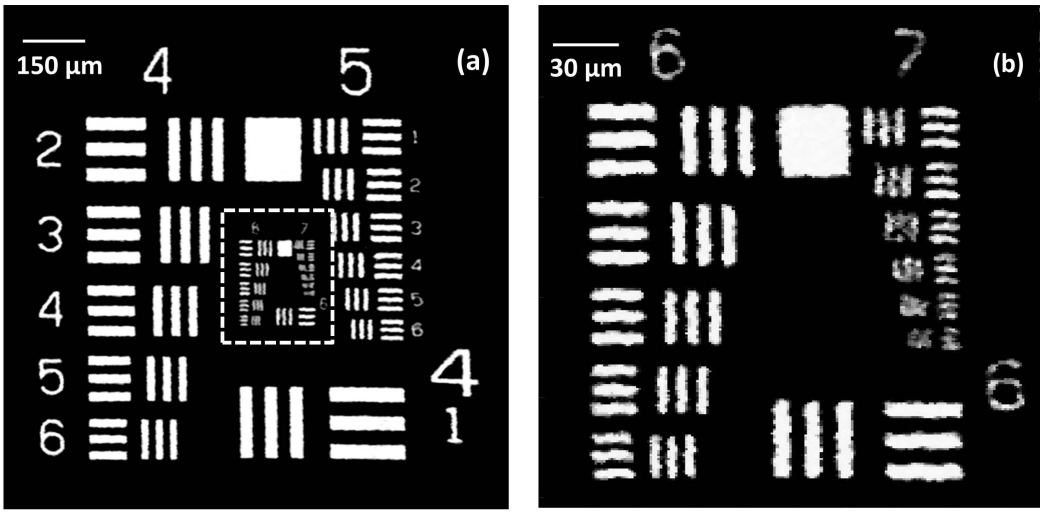

Fig. 2. Lateral resolution test of the OR-PAM system: (a) OR-PAM image of an Air force resolution test target, (b) OR-PAM image of the region of interest (white dotted area in (a)).

Biomedical Optics EXPRESS

Further validation on lateral resolution of the system was done from the full width at half maximum (FWHM) of the line spread function (LSF). The same B-line of a sharp edge of the resolution test target was scanned 50 times with a step size of 0.5 µm. The edge was selected in such a way that during the B-scan half of the image will be contributed by signals from the test target and half will be no signal area from the glass plate. The maximum amplitude projection (MAP) data across the edge (Inlet in Fig. 2(a)) was fitted using the edge-spread function (ESF). By taking the first derivative of ESF the LSF was obtained. The calculated lateral resolution was 3.5 µm as shown in Fig. 3(a) well matching with the previously determined value.

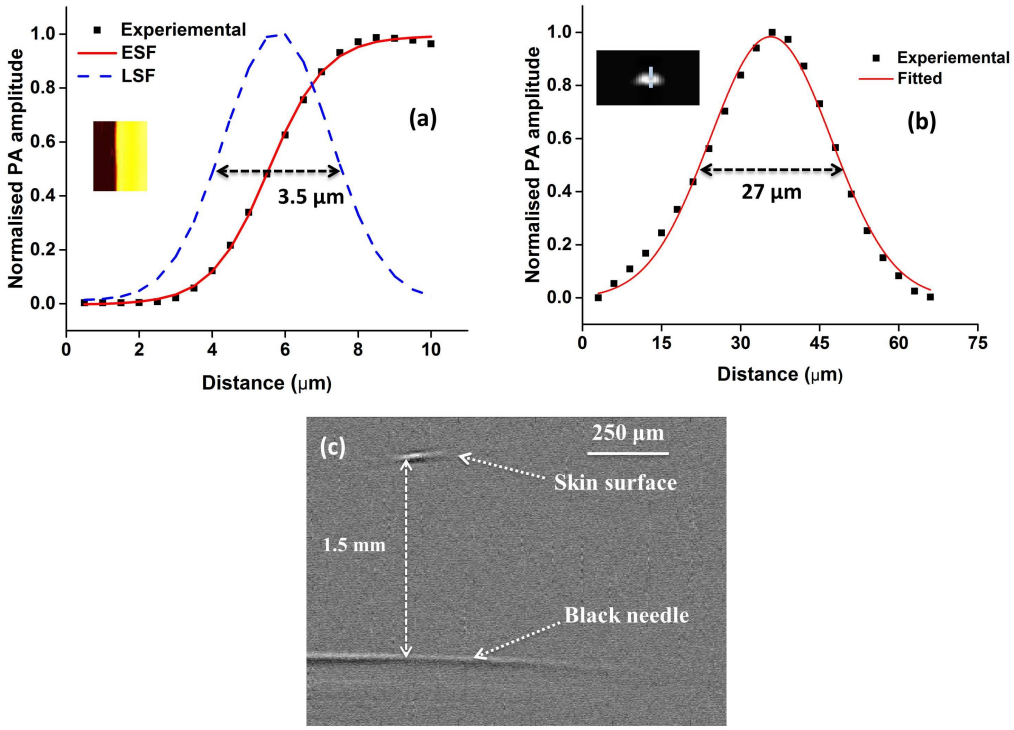

Fig. 3. Spatial resolution and imaging depth test of the OR-PAM system: Measurement of the line spread function (LSF) using the edge of a USAF resolution target. Black (■) dots: photoacoustic signal; red line: edge spread function (ESF); blue line: line spread function (LSF): Inlet shows MAP image of a resolution target (b) photoacoustic axial line of a 6 µm carbon fiber, Inlet shows the B-scan axial image of the carbon fiber (c) Single B-scan PA image of a black needle inserted in a chicken tissue.

Experimentally determined lateral resolution was slightly worse compared to the theoretical resolution of 2.7 µm, which might be due to wavefront aberration due to multiple reflections at the prism interface and MEMS surface. The experimentally determined resolution was good enough to resolve a single capillary. The photoacoustic axial profile from a 6 µm carbon fiber was used to determine the axial resolution of the system. A single carbon fiber was fixed on to a microscopic glass slide with the help of magnifying glass and strapped at the edges. The axial resolution determined from Gaussian fitted LSF of the carbon fiber was 27 µm that closely matches with the theoretical axial resolution of 26 µm. To determine the maximum imaging depth using the proposed system a black needle obliquely inserted on into a chicken tissue was imaged using pulse energy of 400 nJ. Figure 3(c) shows a single B-scan PA image of the needle. The black needle was clearly visible down to ~1.5 mm beneath the tissue surface with a signal-to-noise ratio (SNR) of 8 dB.

Biomedical Optics EXPRESS

Experiments were done using a single mode (SM) fiber (P1-460B-FC-1, Thorlabs) to have a comparison between the SM and MM fiber for OR-PAM applications. A SM fiber (P1-460B-FC1) with a core size of 3.2 µm was used. MM fibers with different core sizes (10 µm and 25 µm) were used for this comparison. Experiments were done to compare the lateral resolution, signal-to-noise ratio (SNR) and *in vivo* imaging depth between SM and MM fibers. The lateral resolution was determined by scanning the edge of the sharp edge of the resolution test target as described before. The measurements were done from the same acoustic focal plane as that of the MM after confirming the optical and acoustic confocal arrangement. The determined lateral resolution using SM fiber was 3.2 µm. For the 10 µm and 25 µm core fibers, the lateral resolution determined was 3.5 µm and 4.9 µm respectively. The lateral resolution of both MM fibers was good enough to resolve single capillaries. In order to determine the SNR, the averaged signal from a 6 µm carbon fiber was taken at a pulse energy of 170 nJ using both SM and MM fiber. The SNR was calculated from 20 $\log_{10}$ ratio of PA signal amplitude to the standard deviation of the noise. The SNR determined from the SM fiber was 47dB whereas from the 10 µm and 25 µm core MM fibers were 44 dB and 39 dB respectively. To determine *in vivo* imaging depth, a golden coloured needle was inserted into the upper leg portion of a normal Balb/c mouse weighing 25 g, procured from InVivos Pte. Ltd. Singapore. All the regulatory guidelines by the institutional Animal Care and Use committee of Singapore Bioimaging Consortium, A*STAR, Singapore (IACUC #151085) were followed for animal experiments. A mixture of Ketamine (120 mg/kg) and Xylazine (16 mg/kg) was used to anesthetize the animal. 0.1 ml/10 gm of the cocktail was injected intraperitoneally. A pulse energy of 400 nJ was delivered using both SM and MM fibers. A narrow blue colour line was drawn at regular intervals on the skin surface of the animal in order to determine the surface position. The imaging depth observed using SM fiber was 0.835 mm whereas using the 10 µm and 25 µm MM fibers were 0.825 and 0.822 mm respectively. It was observed that the use of MM fibers for OR-PAM applications was comparable with SM fiber usage in terms of resolution. The slight difference in SNR might be due to the variations in the optical focus spot sizes and experimental imperfections. In order to determine the power handling capability of the proposed fibers, best coupling efficiency of 70% was achieved at low power using both SM and MM fibers at 10 kHz. With increasing power at the SM fiber input we observed that SM fiber output power also increases maintaining the coupling efficiency and reduced drastically by delivering average power > 25 mW at the input which was due to fiber damage. Whereas the 25 µm MM fiber can withstand a damage threshold > 60 mW. The tabulated comparison between SM and MM fibers is shown in Table 1.

Table 1. Comparison between single mode and multimode fibers

Fiber Type (Core Size)	Lateral Resolution (µm)	SNR (dB)	Imaging depth (µm)
SM Fiber (3.2 µm)	3.2	47	835
MM fiber (10 µm)	3.5	44	825
MM fiber (25 µm)	4.9	39	822

A mouse ear was imaged in order to show the *in vivo* imaging capability at high resolution and high speed using the system. The mouse ear was positioned in a glass slide and was made in close contact with the polyethylene membrane at the bottom of the water tank by means of ultrasound gel. Using the combination of MEMS scanner and mechanical stages a large area (4.8 mm × 5mm) of the ear was first imaged, using a 10 µm MM fiber at a step size of 5 µm in the X and Y direction. The laser repetition rate (LRR) was set at 10 kHz. Four data sets (each of 1.2 × 5mm) were captured and stitched together. The total acquisition time was 4 minutes (Fig. 4(a)). A small area (1.5 mm × 3mm) was scanned using a 25 µm MM fiber at

Biomedical Optics EXPRESS

an LRR of 30kHz using a step size of 5 µm in both X and Y direction. The acquisition time was 15 Seconds. We can clearly see single capillaries from the OR-PAM images. Even though MM fiber can be used at higher repetition rates than 30kHz, the speed of the mechanical stage is the current limiting factor for further improving the imaging speed of the system. The laser pulse energy for all *in vivo* experiments was maintained below American National Standard Institute (ANSI) safety limit of 20 mJ/cm^2.

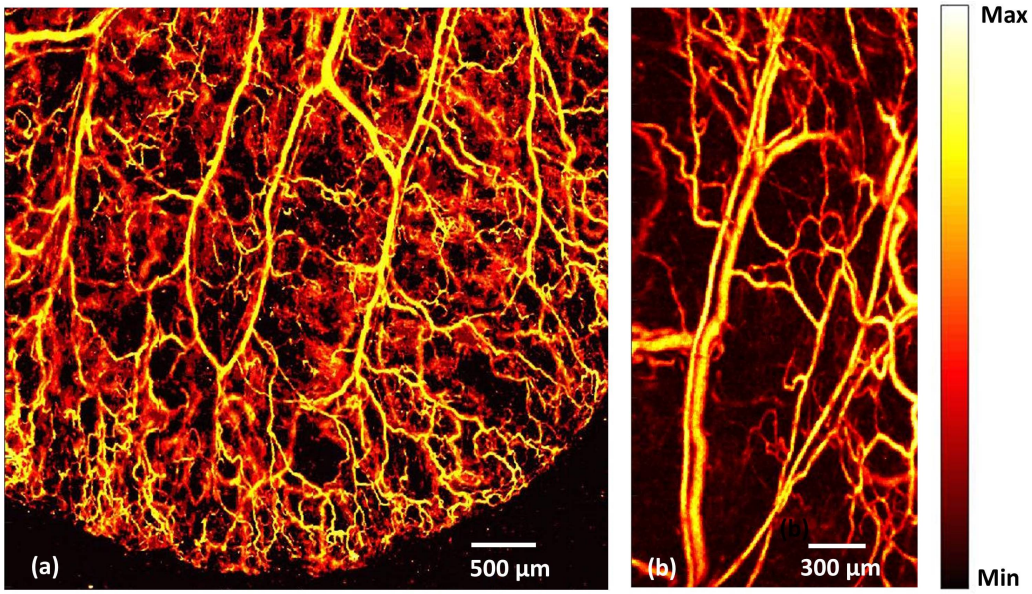

Fig. 4. *In vivo* photoacoustic image of mouse ear: (a) OR-PAM image, using a 10 µm MM fiber at 10 kHz LRR (b) OR-PAM image, using a 25µm MM fiber at 30 kHz LRR.

In order to have a comparison between SM and MM fiber use for *in vivo* imaging, same area of the mouse ear was imaged using both SM and MM fibers. Figure 5(a) shows the area imaged using SM fiber and Fig. 5(b) and 5(c) shows the area images using 10 µm and 25 µm MM fibers. From the images, we can see that the MM fiber image quality is as good as SM fiber image quality, hence MM fibers could be used as a replacement for SM fiber light delivery for OR-PAM imaging applications.

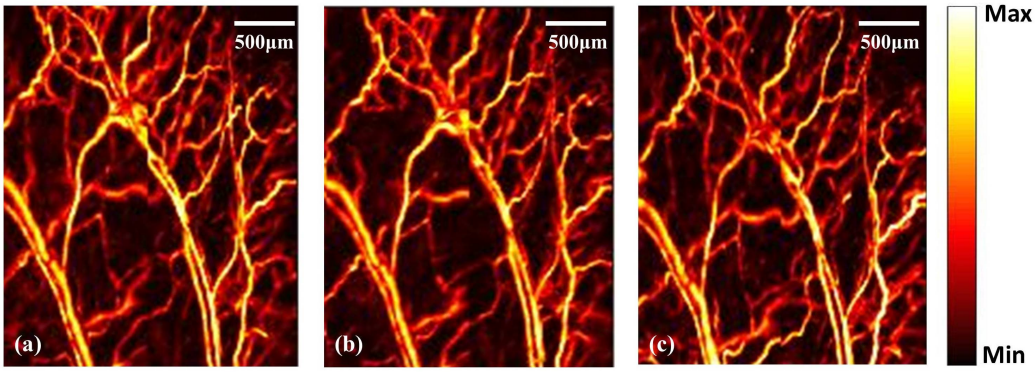

Fig. 5. *In vivo* photoacoustic image of mouse ear using: (a) SM fiber, (b) 10 µm MM fiber (c) 25 µm MM fiber.

In summary, we have demonstrated for the first time the use of MM fibers for high resolution OR-PAM imaging. The proposed system can achieve tight optical focusing using

Biomedical Optics EXPRESS

MM fiber beam excitation and high-speed wide area imaging by utilizing a MEMS scanner and raster mechanical stage movement. The use of a multimode fiber for optical beam delivery allows the system to be user-friendly in terms of fiber coupling and alignment. The high power handling capability of MM fibers makes it ideal for high speed OR-PAM imaging applications as well as for broadband wavelength range imaging applications. The comparative studies on the lateral resolution, SNR and imaging depth between SM and MM fibers show that MM fibers have characteristics closely matching to SM fibers for OR-PAM imaging applications. The use of multimode fibers for high-resolution imaging will be useful in developing high-resolution PAE system which can easily be combined with other optical endoscopic imaging modalities.

4. Conclusions

Here we report for the first time the use of multimode fibers as the optical excitation source for OR-PAM *in vivo* imaging applications. A high-speed OR-PAM system based on a MEMS scanner and MM fiber beam delivery, which can achieve high resolution and wide area scanning, is demonstrated. The system can achieve 3.5 µm lateral resolution and 27 µm axial resolution with 1.5 mm imaging depth. The developed system can be used for high-speed pre-clinical imaging applications. Performance comparison between SM and MM fibers in imaging mode shows that all the parameters for MM fibers including lateral resolution, SNR, and imaging depth are closely matching to that of SM fiber and hence the proposed MM fibers would be ideal for high-speed OR-PAM imaging applications. Furthermore, the use of multimode fibers will be useful in developing high-resolution PAE system and can easily be combined with other optical endoscopic imaging modalities. Studies on the effect of higher mode field diameter MM fibers for OR-PAM will be implemented in our ongoing study.

Funding

Singapore Bioimaging Consortium Intramural Funding, Biomedical Research Council of Agency for Science, Technology, and Research (A*STAR), Singapore; Korea Health Technology R&D Project (HI15C1817) through the Korea Health Industry Development Institute of the Ministry of Health & Welfare, the ICT Consilience Creative Program (IITP-2017-R0346-16-1007) through Institute for Information & communications Technology Promotion of Ministry of Science and ICT; Engineering Research Center Project (2011-0030075) through the National Research Foundation, Republic of Korea.

Acknowledgements

The authors would also like to acknowledge Dr. Ghayathri Balasundaram for valuable discussion and help regarding *in vivo* needle insertion. Dr. Dinish U.S for proofreading the manuscript.

Disclosures

The authors declare that there are no conflicts of interest related to this article. C. Kim and J. Kim have financial interests in PAMsTECH, which, however, did not support this work.